Soft Matter

RSC Publishing

PAPER

View Article Online
View Journal | View Issue

Cite this: *Soft Matter*, 2013, **9**, 9780

Engineering polymeric composite particles by emulsion-templating: thermodynamics *versus* kinetics†

Tiantian Kong,[ab] Zhou Liu,[a] Yang Song,[a] Liqiu Wang*[ab] and Ho Cheung Shum*[ac]

Received 28th April 2013
Accepted 22nd August 2013

DOI: 10.1039/c3sm51176f

www.rsc.org/softmatter

We investigated the important factors that control the structure of polymeric particles fabricated from emulsion templates. We found that the most energetically stable structure predicted by interfacial energy analysis is not always achieved. The slow dynamics due to an increase in the viscosity of the emulsion phases prevents the polymeric particles from achieving their equilibrium structure. We devised a novel strategy to remove this kinetic barrier, thus achieving the expected equilibrium structure. By considering both the thermodynamic and kinetic aspects during the droplet evolution process, a spectrum of final particle structures can be manipulated in a controlled manner. Our work will enable particle engineering for applications including drug delivery, biomimetic vesicles and photonics.

1. Introduction

Due to their tunable size, structure and surface properties, polymer particles find important applications in chromatographic separation, clinical diagnosis, photonics, and drug delivery.[1–10] The performance of polymer particles is strongly influenced by their structures. For example, the solid shells of particles with core–shell structures can protect the active ingredients in the cores against undesired degradation and release to the surroundings.[7,8,10–18] Moreover, the shell layer can also modulate the release pattern of the active ingredients.[12–14] With their two regions of distinctive compositions, Janus particles can provide two compartments for encapsulating two active ingredients of drastically different characteristics and releasing them simultaneously.[19–24] In these applications, the ability to control the structure is critical.

One frequently used and facile method to fabricate polymeric particles is to evaporate the solvent from emulsion droplets.[10,13,25,26] The polymer is first dissolved in a solvent and subsequently used as a dispersed phase to generate emulsions. Generally, spherical polymeric particles are formed since droplets tend to adopt a spherical shape to minimize the overall surface energy. If multiple incompatible compounds are dissolved, phase separation can occur upon the removal of solvents.[24,27–30] The resultant polymeric particles can have a variety of structures, which can be spherical with multiple patches, Janus-like, core–shell or multi-compartmental with detachable compartments.[14,18,26,31,32] Conventionally, the final structure of the formed particles is predicted by analyzing interfacial tensions between various pairs of liquid phases, such as oil, water, or polymer solutions. The structure with the lowest surface energy normally represents the equilibrium structure. So far, this approach has been successful in predicting the final structures of polymer particles prepared.[11,15,17,32] For example, by dissolving a polymer, such as poly(methyl methacrylate) (PMMA) or polystyrene, in a mixture of good and poor organic solvents, polymer shells with oil cores are formed by appropriately adjusting interfacial tensions between immiscible liquids. This core–shell structure, as successfully predicted based on an interfacial tension analysis, with oil phases encapsulated by polymer shells, has been used in ultrasound contrast agents and for controlled release of fragrances.[11,15,17]

However, in polymeric composite particles, which typically consist of polymers and other components, such as surfactants, the final structures of the particles do not necessarily agree with the equilibrium structures predicted.[31,32] Co-existence of several non-equilibrium structures, such as acorn-like and core–shell structures, is also observed.[31,32] The deviation of the final structures from the equilibrium structure predicted is not unique to polymeric particles. In the self-assembly of amphiphilic molecules, such as lipids and block copolymers, different non-equilibrium structures are often observed. Due to trapping of the molecules by the preparation conditions, the final structures often depend more on the processing path these molecules take towards equilibrium.[29,33,34] These observations suggest that thermodynamics is not the only factor that controls the final structures of multiphase systems. Similarly, as emulsion droplets solidify into particles, fluid properties such as viscosity change dramatically. As viscosity increases, the solidification dynamics may slow down and prevent the equilibrium

[a]*Department of Mechanical Engineering, The University of Hong Kong, Pokfulam Road, Hong Kong. E-mail: ashum@hku.hk; lqwang@hku.hk*

[b]*HKU-Zhejiang Institute of Research and Innovation (HKU-ZIRI), Hangzhou, 311100, Zhejiang, China*

[c]*HKU-Shenzhen Institute of Research and Innovation (HKU-SIRI), Shenzhen, 518000, Guangdong, China*

† Electronic supplementary information (ESI) available. See DOI: 10.1039/c3sm51176f

structure to be reached. This kinetic aspect of the droplet evolution remains to be explored. Thus, a comprehensive understanding of the important factors contributing to the final structure will enable us to avoid the generation of non-equilibrium structures and manipulate the final structures in a controlled manner.

In this work, we investigate the kinetic and thermodynamic conditions during emulsion droplet solidification, and their effect on the final structures of the polymer particles. We show that the equilibrium structures cannot always be achieved and kinetic parameters controlled by viscosity also have to be considered. To confirm the importance of the kinetic aspect, we demonstrate that by removing the kinetic barrier, the equilibrium morphology can be achieved. An understanding of the balance between thermodynamic and kinetic conditions enables control over the microstructures and functionality of polymer particles. This provides a convenient and robust tool to predict and tailor the structures of multi-phase systems to meet the specific needs of the applications of interest.

2. Experimental

We use a capillary microfluidic device to generate monodisperse oil-in-water single emulsions.[2,7,16,18,21,23,24,27,28,30,35–37] In a typical capillary microfluidic device, two cylindrical capillaries (World Precision Instrument Inc.), which have inner and outer diameters of 0.58 mm and 1 mm respectively, are tapered using a micropipette puller (P-97, Sutter Instrument, Inc.). The tips of the capillaries are polished to desired diameters using sandpaper. Typical tip diameters of the injection and collection capillaries are 25 μm and 100 μm, respectively. Then the polished round capillaries are coaxially aligned inside a square capillary (AIT glass). Monodisperse single emulsions can be generated using either a co-flow or flow-focusing geometry.

To prepare single emulsion droplet templates, we dissolve a polymer, poly(lactic-*co*-glycolic acid) (PLGA 50 : 50), and a surfactant, namely Dow Corning 749 fluid or sorbitan monooleate (span 80), in dichloromethane (DCM), which is a good solvent for PLGA. The mixture is used as the dispersed phase. The concentration of the polymer and surfactant can be varied to control the size of the compartments of the resultant microparticles. Deionized water with 10% (w/v) poly(vinyl alcohol) (PVA) is used as the outer continuous phase. PVA acts as an emulsifier to prevent oil droplets from coalescence. To speed up the phase separation in the droplet phase, 0.2 wt% fluorescein sodium salt is added to PVA solution, which forms the outer continuous phase. Monodisperse single emulsion droplets of DCM with the polymer and surfactant are generated in a continuous phase of PVA solution using the single-emulsion microfluidic device. The flow rates of the dispersed and the continuous phases in all experiments are fixed at 400 and 4000 μl h^{-1} respectively.

The phase separation of the emulsion droplet is recorded using a high speed camera (Redlake, MotionPro X4). The morphology of resultant microparticles is characterized using an optical microscope (Motic 3000) and a variable pressure scanning electron microscope (Hitachi S3400N VP-SEM). The contact angle between the separating droplets is obtained by analyzing microscope images using an open-source image analysis software, Image J.

3. Results and discussion

Phase separation between the polymer and surfactant in emulsion microdroplets is observed when the solvent diffuses out of the droplets and evaporates.[38] As soon as emulsion droplets are collected from the microfluidic device (Fig. 1(a) and (b)), the solvent, dichloromethane, diffuses into the aqueous continuous phase. This leads to a decrease in droplet volume by

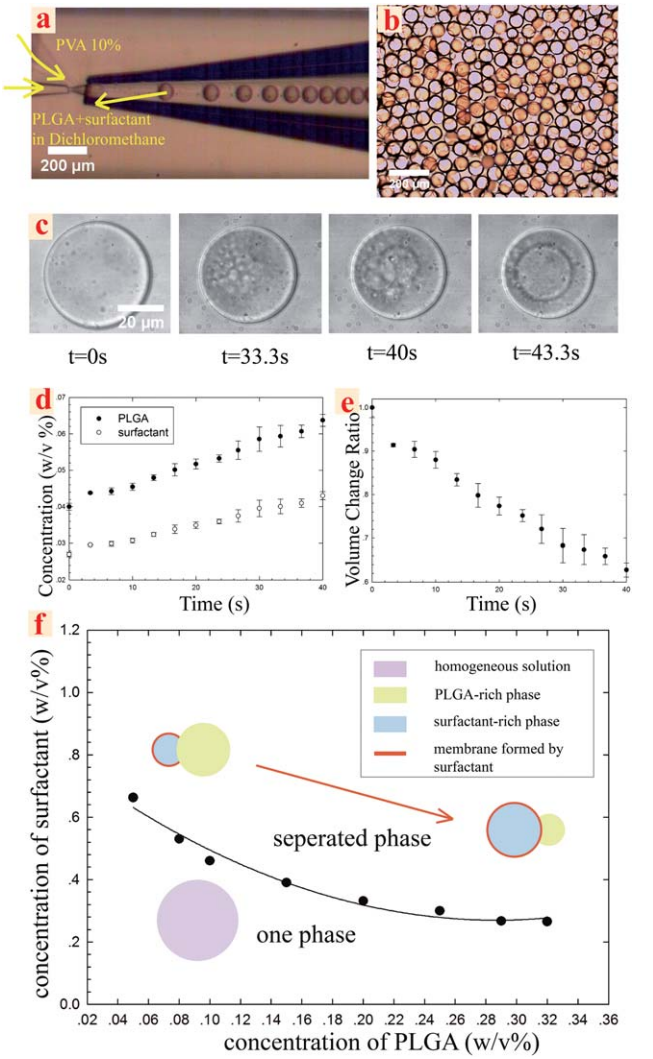

Fig. 1 Optical microscope images showing (a) microfluidic generation of monodisperse single emulsion droplets and (b) collection of monodisperse O/W emulsion droplets. (c) Series of optical micrographs showing the phase separation inside an emulsion droplet. (d) Plot of droplet volume change as a function of time: the droplet volume change ratio is defined as the droplet volume at a given time t divided by the initial droplet volume at time $t = 0$. (e) Plot of concentration of PLGA and surfactant as a function of time. (f) Phase diagram of PLGA and surfactant in dichloromethane; PLGA and Dow Corning 749 fluid are dissolved at various concentrations in dichloromethane, and the resultant solutions containing PLGA and Dow Corning 749 are subsequently examined to detect any separation into two immiscible phases under the prescribed compositions.

nearly 40% within 40 seconds, as shown in Fig. 1(c) and (d), and thus an increase in the concentration of both polymer and surfactant, as shown in Fig. 1(e). The increase in concentrations induces phase separation seconds after the collection of oil droplets. Small droplets appear inside the emulsion droplet, which consists of a mixture of PLGA, surfactant and dichloromethane. Subsequently, the small droplets grow and coalesce into one big droplet, as demonstrated by the formation of a blurry oil–oil (O/O) interface shown in Fig. 1(c). As a result, an oil-in-oil-in-water (O/O/W) double emulsion droplet is formed, with the core and shell phases being dichloromethane concentrated in PLGA and surfactant respectively. When phase separation occurs within an emulsion microdroplet, the concentrations of PLGA and surfactant in dichloromethane are estimated to be 6.37×10^{-2} g ml^{-1} and 4.3×10^{-2} g ml^{-1}, respectively. However, at these concentrations, the mixture of PLGA and surfactant should form one phase in dichloromethane, instead of two separate phases, according to the phase diagram in Fig. 1(f). In our experiment, phase separation in the emulsion droplet is observed at concentrations about 15 times lower than expected. The occurrence of phase separation at such low overall surfactant and polymer concentrations could be due to the accumulation of surfactants at the oil/water interface, increasing the effective concentration; this can lead to the precipitation of surfactants from the PLGA-rich dichloromethane phase.

The emulsion configuration with the lowest surface energy is believed to be the most thermodynamically stable. To predict the equilibrium structure, we calculate the Gibbs free energy $G = \Sigma A_{ij}\gamma_{ij}$ of the core–shell droplet and of two separated oil droplets; if the interfacial tension between the core and the shell phases is larger than the difference between the core/continuous and shell/continuous interfacial tension, $\gamma_{12} > \gamma_{13} - \gamma_{23}$, the configuration of two separated oil droplets is thermodynamically favored. For the initial oil-in-oil-in-water double emulsion droplet, γ represents the interfacial tension, and "1", "2", and "3" denote the core phase, the shell phase and the aqueous continuous phase, respectively, as shown in Fig. 2. In our experiment, $\gamma_{13} - \gamma_{23}$ is a constant with a value of 0.3 mN m^{-1}, since the interfacial tensions are not expected to change with the increase in the concentration of either PLGA or surfactant, as shown in Table S1.† However, γ_{12} increases as the concentration of PLGA and surfactant increases, as suggested by the increasingly clear oil–oil interface in Fig. 3(a) and (b). We choose two phases, 0.48 g ml^{-1} PLGA in dichloromethane and 0.32 g ml^{-1} surfactant in dichloromethane, which should resemble the compositions of phases 1 and 2 in the emulsion droplets as they start solidifying; the equilibrium interfacial tension between the two phases is measured to be 0.6 mN m^{-1}, which is larger than the value of $\gamma_{13} - \gamma_{23}$. Therefore, the configuration in which the core and shell phase are completely separated will be the most thermodynamically stable, and thus is predicted to be the equilibrium configuration.

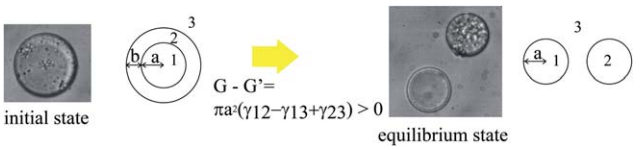

Fig. 2 Schematic of the initial (left) and equilibrium (right) states of emulsion configuration.

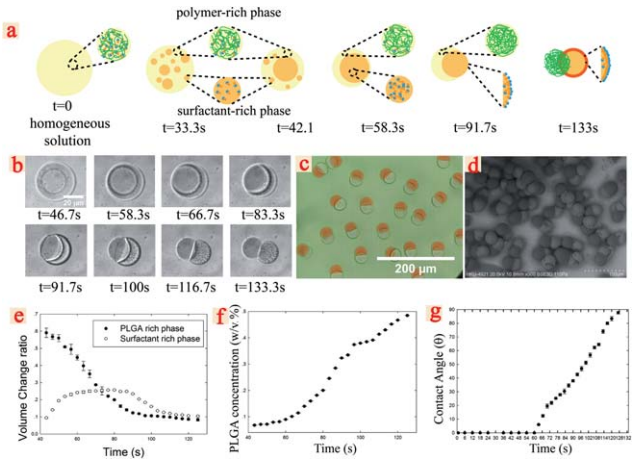

Fig. 3 (a) Schematic of the formation of an acorn-like microparticle from a single emulsion droplet. (b) Series of optical micrographs showing the dewetting of the core phase from the shell phase. (c) Optical microscope image of acorn-like microparticles with one compartment being a PLGA microsphere and one compartment being a capsule formed by the precipitation of surfactants. The yellow color in one compartment is due to the presence of a hydrophobic drug, rifampicin, which is encapsulated in PLGA matrices. (d) VP-SEM image of acorn-like microparticles. (e) Plot of the volume change of PLGA-rich and surfactant-rich phases as a function of time. (f) Plot of the PLGA concentration in the PLGA-rich phase as a function of time. (h) Plot of the contact angle of PLGA-rich and surfactant-rich droplets as a function of time.

Surprisingly, instead of two completely separated droplets, acorn-like microparticles form (Fig. 3(a)–(d)). Dewetting induces the shell phase to collect on one side of the core droplet; subsequent solidification leads to the formation of acorn-like microparticles with two distinct compartments, as illustrated in Fig. 3(a) and shown in Fig. 3(c) and (d). After the formation of the O/O/W droplet at $t = 43.3$ s, from $t = 46.7$ s to $t = 58.3$ s, the core phase of surfactant-rich dichloromethane continues to separate from the shell phase of PLGA-rich dichloromethane, resulting in an increase of core size as shown in Fig. 3(e). From $t = 66.7$ s to 80 s, phase separation reaches equilibrium and thus the core size remains the same (Fig. 3(e)). After 80 s, the surfactant-rich dichloromethane droplet shrinks due to solvent evaporation, as shown in Fig. 3(e). Meanwhile, the shell phase also evaporates and starts to move away from the core phase (Fig. 3(b) and (e)). The shrinkage of the shell phase, PLGA-rich dichloromethane, leads to a ten-fold increase in the concentration of PLGA from 4×10^{-2} g ml^{-1} to 0.485 g ml^{-1} (Fig. 3(f)). Thus, the viscosity of the shell phase increases by more than 12 times (Fig. S2†). The increase in viscosity leads to a reduction in the speed at which the two droplets separate. As a result, the structure of the dewetting droplets is frozen, leading to the formation of a non-equilibrium acorn-like particle with a contact angle, θ, of 90°, as shown in Fig. 3(g). One side of the

acorn-like particle is made up of PLGA while the other side is a capsule formed by the precipitation of surfactants at the interface. The surfactants in the dispersed phase can precipitate at the O/W interface to form a capsule with an oil phase encapsulated inside; this is demonstrated in Fig. S3 and Video S4.† Our particles have an acorn-like structure with the two compartments remaining attached even after over two months.

If the increase in viscosity indeed accounts for the inability to achieve complete separation of the two oil droplets, which has been predicted by thermodynamic considerations, by forcing the viscosity to remain low during the separation, complete separation should be achievable. The viscosity of the shell phase is determined by the volume fraction of PLGA, which increases as the droplet volume decreases over time due to evaporation of dichloromethane. Therefore, the viscous barrier should be lowered if the phase separation process is sufficiently accelerated. To achieve this, we add to the continuous phase a salt that preferentially dissolves in only one of the two phase-separated oil phases (Fig. S5†). The addition of salt does not alter the O/W interfacial tension or the viscosity of the polymer-rich phase, but increases the phase separation speed,[39] and thus the speed at which the two oil phases move apart is also accelerated, as illustrated in Fig. 4(a) and (b). As soon as the oil-in-oil droplet is formed at $t = 40$ s, the core droplet size does not change until it is completely detached from the PLGA rich droplet, as shown in Fig. 4(b) and (d). The constant size of the core suggests that phase separation between PLGA and surfactant is completed before $t = 40$ s, which is almost 50 seconds earlier than the previous case in the absence of the salt with selective solubility,

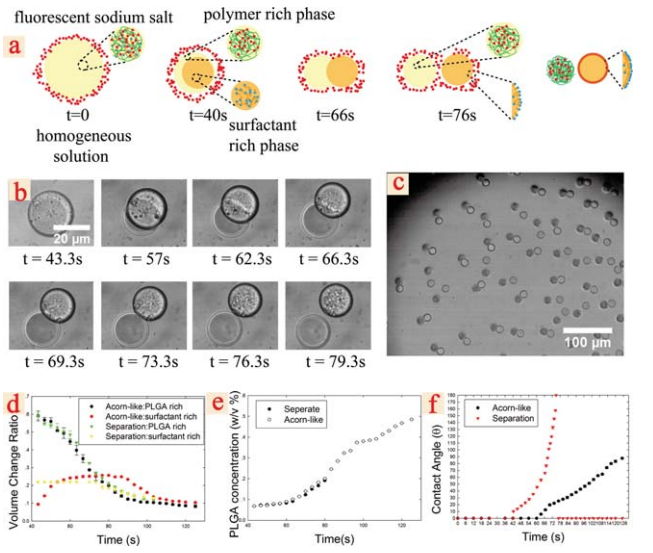

Fig. 4 (a) Schematic of the formation of two completely separated microparticles from a single emulsion droplet. (b) Series of optical micrographs showing the detachment of the core phase from the shell phase. (c) Optical microscope image of two completely separated microparticles, namely, a PLGA microparticle and a capsule formed by the precipitation of the surfactants. (d) Plot of the volume change of the PLGA-rich and surfactant-rich phases as a function of time. (e) Plot of the PLGA concentration in the PLGA-rich dichloromethane phase as a function of time. (f) Plot of the contact angle of the PLGA-rich and surfactant-rich droplets as a function of time. The salt concentration in the continuous phase is 0.2 wt%.

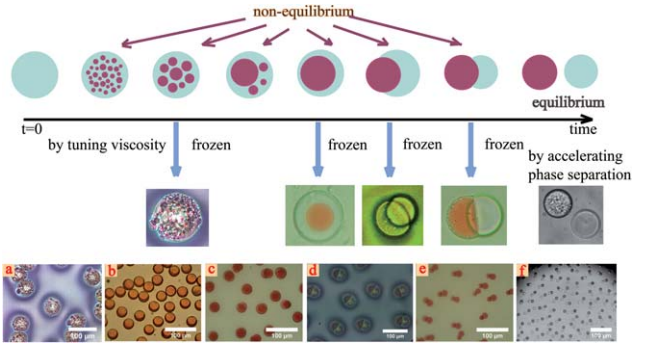

Fig. 5 Schematic of the full spectrum of microparticle structures from a single emulsion droplet. Optical microscopic images of (a) microparticles with multiple patches, (b) core–shell microparticles with oil cores, (c–e) acorn-like microparticles with various contact angles of two compartments and (f) two completely detached compartments.

as shown in Fig. 4(d). The period of the whole detaching process is about 2.36 times shorter than that for the case resulting in acorn-like structures (Fig. 4(b) and (d)); therefore, the concentration of the shell phase, PLGA-rich dichloromethane, only rises to 0.16 g ml^{-1}, which is about 3 times lower than that without the salt, as shown in Fig. 4(e). Thus the viscosity of PLGA-rich dichloromethane is almost 4 times lower than that without the salt immediately after the droplet separation process is completed. As a result, the two droplets are able to move away from each other, as shown by comparing the corresponding changes in contact angle with time in Fig. 4(f). From $t = 76.3$ s onwards, these two separated droplets shrink in size due to solvent evaporation (Fig. 4(d)), and subsequently solidify into two separate spherical particles (Fig. 4(b) and (c)), with one being a PLGA microsphere and the other being a capsule with a shell layer of precipitated surfactants. Thus, the added salt accelerates the separation process and the two droplet phases have sufficient time for complete detachment from each other before they are solidified within minutes. Our results confirm our hypothesis that slow dynamics due to increased viscosity can serve as a kinetic barrier that prevents the formation of the thermodynamically favoured equilibrium structures, and this barrier can be avoided by accelerating the phase separation process.

The understanding of both the thermodynamic and kinetic aspects enables control over a range of structures, including spherical with multiple patches, core–shell, Janus-like and bi-compartmental with a detachable compartment, from a single emulsion droplet, as demonstrated in Fig. 5.

4. Conclusions

In this work, we demonstrate that kinetic aspects during the evolution of emulsion droplet structures are important for determining the structure of polymeric microparticles fabricated from emulsion templates. Phase separation occurs between incompatible compounds upon the removal of solvents, and causes the structures of the resultant particles to evolve. Our results show that the final structures do not always

follow thermodynamic prediction; kinetic factors can also play a critical role, as demonstrated by the slowing down of droplet evolution dynamics due to the increased viscosity of the emulsion phases. By accelerating the phase separation speed, separation of the two droplet phases can be achieved before their viscosities get too high; thus the kinetic barrier can be removed. The understanding of the balance between the kinetic and thermodynamic factors during emulsion evolution allows us to achieve a range of structures in a controlled manner. It provides a robust approach for predicting and tailor-designing desired structures of multiphase particle systems to fulfill the specific needs of the applications of interest. The ability to detach one compartment from the other by tuning the phase separation speed is especially useful in the fabrication of material systems, such as liposomes and polymersomes, that involve surface-active components from emulsion templates.

Acknowledgements

We gratefully acknowledge financial support from the Research Grants Council of Hong Kong (HKU717613E, HKU718111E and HKU718009E), the Science and Technology Innovation Commission of Shenzhen Municipality (JC201105190878A), the National Natural Science Foundation of China (NSFC51206138/E0605) as well as the Seed Funding (201109160030 and 201109176165) and the University Development Fund from The University of Hong Kong . This research is also supported in part by the Zhejiang Provincial, Hangzhou Municipal and Lin'an County Governments.

Notes and references

1 C. Paquet and E. Kumacheva, *Mater. Today*, 2008, **11**, 48–56.
2 S. Ma, J. Thiele, X. Liu, Y. Bai, C. Abell and W. T. S. Huck, *Small*, 2012, **8**, 2356–2360.
3 S. Kim, J.-H. Kim, O. Jeon, I. C. Kwon and K. Park, *Eur. J. Pharm. Biopharm.*, 2009, **71**, 420–430.
4 L. Brannon-Peppas, *Int. J. Pharm.*, 1995, **116**, 1–9.
5 S. Xu, J. Zhang, C. Paquet, Y. Lin and E. Kumacheva, *Adv. Funct. Mater.*, 2003, **13**, 468–472.
6 L. Ye, R. Weiss and K. Mosbach, *Macromolecules*, 2000, **33**, 8239–8245.
7 S. Seiffert, *Macromol. Rapid Commun.*, 2011, **32**, 1600–1609.
8 Y. H. Deng, W. L. Yang, C. C. Wang and S. K. Fu, *Adv. Mater.*, 2003, **15**, 1729–1732.
9 H. Kawaguchi, *Prog. Polym. Sci.*, 2000, **25**, 1171–1210.
10 W. J. Duncanson, T. Lin, A. R. Abate, S. Seiffert, R. K. Shah and D. a. Weitz, *Lab Chip*, 2012, **12**, 2135–2145.
11 E. Pisani, N. Tsapis, J. Paris, V. Nicolas, L. Cattel and E. Fattal, *Langmuir*, 2006, **22**, 4397–4402.
12 Y. Y. Huang, T. W. Chung and T. W. Tzeng, *Int. J. Pharm.*, 1999, **182**, 93–100.
13 S. Freiberg and X. X. Zhu, *Int. J. Pharm.*, 2004, **282**, 1–18.
14 E. M. K. J. Pekarek and J. S. Jacob, *Nature*, 1994, **367**, 258–260.
15 R. Atkin, P. Davies, J. Hardy and B. Vincent, *Macromolecules*, 2004, **37**, 7979–7985.
16 C.-H. Choi, J.-H. Jung, D.-W. Kim, Y.-M. Chung and C.-S. Lee, *Lab Chip*, 2008, **8**, 1544–1551.
17 P. J. Dowding, R. Atkin, B. Vincent and P. Bouillot, *Langmuir*, 2004, **20**, 11374–11379.
18 C.-H. Choi, D. A. Weitz and C.-S. Lee, *Adv. Mater.*, 2013, **25**, 2536–2541.
19 K. Roh, D. C. Martin and J. Lahann, *Nat. Mater.*, 2005, **4**, 759–763.
20 J. a. Champion, Y. K. Katare and S. Mitragotri, *J. Controlled Release*, 2007, **121**, 3–9.
21 C.-H. Chen, R. K. Shah, A. R. Abate and D. a. Weitz, *Langmuir*, 2009, **25**, 4320–4323.
22 S. Seiffert, M. B. Romanowsky and D. a. Weitz, *Langmuir*, 2010, **26**, 14842–14847.
23 N. Prasad, J. Perumal, C.-H. Choi, C.-S. Lee and D.-P. Kim, *Adv. Funct. Mater.*, 2009, **19**, 1656–1662.
24 R. K. Shah, J.-W. Kim and D. A. Weitz, *Adv. Mater.*, 2009, **21**, 1949–1953.
25 H. Jeffery, S. S. Davis and D. T. O'Hagan, *Int. J. Pharm.*, 1991, **77**, 169–175.
26 I. D. Rosca, F. Watari and M. Uo, *J. Controlled Release*, 2004, **99**, 271–280.
27 H. C. Shum, E. Santanach-Carreras, J.-W. Kim, A. Ehrlicher, J. Bibette and D. a. Weitz, *J. Am. Chem. Soc.*, 2011, **133**, 4420–4426.
28 S.-H. Kim, A. Abbaspourrad and D. a. Weitz, *J. Am. Chem. Soc.*, 2011, **133**, 5516–5524.
29 R. C. Hayward and D. J. Pochan, *Macromolecules*, 2010, **43**, 3577–3584.
30 R. C. Hayward, A. S. Utada, N. Dan and D. a. Weitz, *Langmuir*, 2006, **22**, 4457–4461.
31 E. Pisani, E. Fattal, J. Paris, C. Ringard, V. Rosilio and N. Tsapis, *J. Colloid Interface Sci.*, 2008, **326**, 66–71.
32 D. C. Sundberg, A. P. Casassa, J. Pantazopoulos, M. R. Muscato, B. Kronberg and J. Berg, *J. Appl. Polym. Sci.*, 1990, **41**, 1425–1442.
33 M. Antonietti and S. Förster, *Adv. Mater.*, 2003, **15**, 1323–1333.
34 M. Li and S. Mann, *Angew. Chem., Int. Ed.*, 2008, 9476–9479.
35 R. K. Shah, H. C. Shum, A. C. Rowat, D. Lee, J. J. Agresti, A. S. Utada, L.-Y. Chu, J.-W. Kim, A. Fernandez-Nieves, C. J. Martinez and D. A. Weitz, *Mater. Today*, 2008, **11**, 18–27.
36 A. S. Utada, E. Lorenceau, D. R. Link, P. D. Kaplan, H. A. Stone and D. A. Weitz, *Science*, 2005, **308**, 537–541.
37 J.-W. Kim, D. Lee, H. C. Shum and D. A. Weitz, *Adv. Mater.*, 2008, **20**, 3239–3243.
38 P. van de Witte, P. J. Dijkstra, J. W. a. van den Berg and J. Feijen, *J. Membr. Sci.*, 1996, **117**, 1–31.
39 H.-O. Johansson, E. Feitosa and A. P. Junior, *Polymers*, 2011, **3**, 587–601.

